Journal of Petroleum Science and Engineering 201 (2021) 108455

Contents lists available at ScienceDirect

Journal of Petroleum Science and Engineering

journal homepage: http://www.elsevier.com/locate/petrol

Alternative setting materials for primary cementing and zonal isolation – Laboratory evaluation of rheological and mechanical properties

Mohammadreza Kamali [a,*], Mahmoud Khalifeh [a], Arild Saasen [a], Rune Godøy [b], Laurent Delabroy [c]

[a] Department of Energy and Petroleum Engineering, University of Stavanger, 4036, Stavanger, Norway
[b] R&D Department, Equinor, 4035, Stavanger, Norway
[c] Aker BP ASA, 4020, Stavanger, Norway

ARTICLE INFO

Keywords:
Drilling operation
Zonal isolation
Primary cementing
Barrier materials
Cementing

ABSTRACT

Portland cement is the prime zonal isolation material used in hydrocarbon wells and its utilization has been extended to geothermal, carbon sequestration and gas storage wells. Despite the vast quantity of research activities and publications, well integrity reports show shortcomings associated with Portland cement at specific conditions of pressure, temperature, chemical environment and geographical locations. In this experimental study, four alternative barrier materials have been selected for further experiments at laboratory scale: an industrial class of expansive cement, a non-cement pozzolanic slurry, a rock-based geopolymer and an organic thermosetting resin. Neat class G cement was used as reference material for comparing the results.

The study includes the rheological behavior of the candidate materials, static fluid-loss and pumpability at both atmospheric and elevated pressures. All of the materials at the liquid phase showed an acceptable viscosity profile at the operational shear rates. The consistency curve of the slurries showed that the barrier materials are pumpable for the desired period with the right-angle set (RAS), except for the pozzolanic slurry, which was not able to make gel up to 24 h at dynamic conditions.

Mechanical properties of the candidate barrier materials including uniaxial compressive strength (UCS), modulus of flexibility, sonic strength development and tensile strength of the samples were characterized up to 28 days of curing. The UCS test results showed that the thermosetting resin has an extremely high compressive strength compared to the other materials, while the geopolymer and the pozzolanic slurry are more ductile. The tensile strength of the materials experienced no significant change over time; however, for the neat class G cement, it is reduced after 28 days.

1. Introduction

During zonal isolation operations, known as primary cementing, Portland cement is normally used as well barrier element to provide well integrity by preventing uncontrolled fluid flow behind the casing string. Portland cement serves the casing by anchoring and protection for a corrosive downhole environment. The barrier material is a key element to maintain well integrity, it should be able to meet a number of criteria necessary to achieve a safe operation during the life cycle of the well. According to the available guidelines (American Petroleum Institute, 2013; American Petroleum Institute, 2017; International Organization for Standardization, ISO, 2014; Norsok, 2013), candidate barrier materials have to make an integrated bonding with the casing pipe and formation to sufficiently seal the annular space between casing and formation or two casings. Additionally, the zonal isolation materials should be impermeable to prevent fluid migration within the barrier sheath. The bottom-hole corrosive environment shall not critically deteriorate the chemical and mechanical properties of the zonal isolation material. The intense mechanical loads are sometimes unavoidable; hence, it is essential that the barrier material has adequate mechanical strength and flexibility to withstand the downhole stresses caused by temperature and pressure changes. In addition, it is necessary to avoid the changes in the bulk volume of the barrier material. Severe shrinkage and expansion in the volume can damage the barrier sheath and consequently, results in loss of well integrity. Lastly, the compatibility of cementitious material and casing should be considered; any detrimental

* Corresponding author.
E-mail address: Mohammadreza.kamali@uis.no (M. Kamali).

https://doi.org/10.1016/j.petrol.2021.108455
Received 5 October 2020; Received in revised form 19 January 2021; Accepted 21 January 2021
Available online 27 January 2021

reaction at the interface can cause debonding and forming micro-annular paths.

Ordinary Portland cement (OPC) has been used extensively for primary cementing operations for many years (Nelson and Guillot, 2006). Therefore, its properties and behavior at various phases are well-known among engineers and academia. Along with its availability and reasonable market price, OPC has been a practical cementitious material for primary cementing, remedial activities and permanent plug and abandonment (P&A) (Le-Minous et al., 2017). However, over the years, a number of concerns related to short- and long-term utilization of OPC has been stated by operating companies and scientists (Jimenez et al., 2016). The industrial reports and academic publications have declared that a range of 2–45% of both production and injection wells, depending on the number of the wells per geographical location, suffer from well integrity issues (Davies et al., 2014; Vignes, 2011). They addressed the major shortcomings like low ductility and brittleness, bulk shrinkage while curing, low durability in a corrosive environment, and low thermal and chemical stability at elevated temperatures (Al Ramadan et al., 2019; Kiran et al., 2017; Vrålstad et al., 2018). Enormous research works have studied the effect of different additives intending to enhancing both rheological and mechanical properties of OPC and make it adaptable to drilling conditions (Jafariesfad et al., 2017a; Khalil et al., 2020; Mangadlao et al., 2015; Moreira et al., 2018). Despite all modifications and researches conducted on development of additives to well cements, the concerns are still valid as the main root of shortcomings is cement chemistry. Therefore, researchers have been searching for alternatives to Portland cement for field applications. Of these, one may refer to expansive cement, Pozzolanic based slurries, geopolymers and thermosetting resins (Abid et al., 2019; Beharie et al., 2015; Jafariesfad et al., 2017b; Khalifeh et al., 2018).

The current objective is to characterize rheological behavior and mechanical properties of the abovementioned materials at the equal downhole condition and presenting their shortcomings and advantages. The mechanical properties were measured in the short-term, and in a time span from 24 h after curing up to 28 days. The result for each test is compared with test results obtained with neat API class G cement, which is the prime material for the OPC. During this project, the bottom-hole circulating temperature (BHCT) was set to 65 °C, while the bottom-hole static temperature (BHST) was 90 °C. The pressure for curing the samples was equal to 17 MPa. This condition is applicable to the majority of the wells on the Norwegian Continental Shelf (NCS). Prior to discussing the experimental results, it is necessary to familiarize readers with barrier materials.

1.1. Expansive cement

Integrated bonding at cement-casing and cement-formation interfaces is crucial for achieving zonal isolation. Cement shrinkage is a result of chemical, autogenous and drying shrinkage phenomena. Hydration reaction of cement is associate with shrinkage as volume of the paste product is less than the reactants (Henkensiefken et al., 2009). The decrease in volume due to the hydration reaction is referred to as chemical shrinkage. The hydration reaction, however, continues as the slurry hardens. The unreacted cement in the system consumes the remaining water trapped in pores and leave the pores empty. The pore water drainage results volume reduction, which is caused by capillary pressure development and extra tension within the cement matrix. This process is simplified in Fig. 1. The volume change due to the pore water consumption is known as autogenous shrinkage. As the slurry solidifies, the change in volume is because of the autogenous shrinkage, which is lower compare to the chemical shrinkage (Henkensiefken et al., 2009). The shrinkage-induced tension can be intensified at the cement sheath inner and/or outer circumferences by external loads from pressure or temperature changes at nearby environment. If the summation of tensions exceeds the tensile strength of the cement, the risk of forming radial cracks or debonding from casing and formation increases significantly.

A proven approach of improving sealability and elimination of micro-annuli formation due to OPC volume shrinkage is the use of expansive zonal isolation materials, which expand upon setting (Baumgarte et al., 1999). The expanding agents act either by making crystals growing within the structure or by the controlled generation of gas bubbles within the cement matrix. Different mechanisms can be taken to acquire expansion within the cement system, and they are extensively reviewed in the literature (Nelson and Guillot, 2006; Santos et al., 2018; Thomas et al., 2014). Among all methodologies that have been investigated, the application of magnesium oxide (MgO) in well cements have revealed appropriate results. In civil and construction industry, where confining pressure may not exist, the amount of MgO is critically controlled to avoid cracks due to the expansion of the cement matrix. In the oil well, on the contrary, MgO can compensate shrinkage and maintain zonal isolation. The effectiveness of the expansive agent reaches a maximum when the corresponding expansion reaction takes place while the shrinkage arises. On one hand, the early expansion would not compensate for the long-term shrinkage in the cement matrix. Very late expansion may cause crack in the cement structure; hence, the expansive additives should be carefully engineered. Yet, the full control of the reaction and the effectiveness of the agent at different operational conditions are under investigation (Santos et al., 2020). The parameters such as expansive agent's particle size, and the dosage, time control of the reaction, and downhole pressure and temperature have a critical role in short- and long-term mechanical properties of the cement after solidification. The experimental observations show that hybrid use of nano-sized MgO with diverse reactivity levels can solve the issue of early expansion before solidification of the cement slurry (Jafariesfad et al., 2017b).

In this research work, a commercial industry expansive cement, which is extensively used for P&A operation is investigated for primary cementing operation and zonal isolation. The cement system has MgO as an expansive agent. This agent is dry blended with API class G cement.

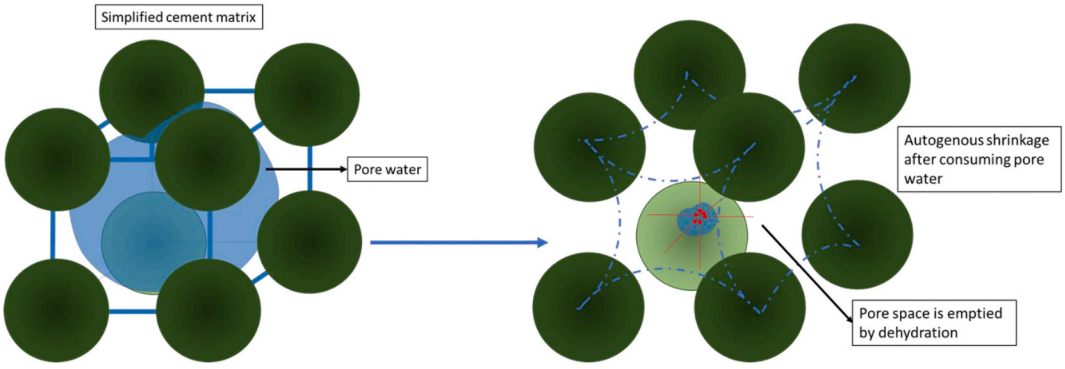

Fig. 1. Autogenous shrinkage of the cement-based materials during solidification.

1.2. Pozzolanic slurry

Some silica-rich materials, known as pozzolans, may not have cementitious properties on their own, but react with calcium hydroxide ($Ca(OH)_2$) in an aqueous environment and show cementitious properties (American Society for Testing and Materials, ASTM, 2013). Pozzolans are widely used as cement extender for cement and they are available in natural and artificial types. In the presence of pozzolans, the permeability of cement is significantly reduced and the silica reacts with undesirable side reaction products, $Ca(OH)_2$ in the system and form a stable and durable calcium – silicate – hydrate (C–S–H) compound. The microporous structural units broadly known as zeolites exist in pozzolanic materials. Zeolites can act as an ion-exchange component in a corrosive environment and maintain the cement properties (Papadakis et al., 1992).

In this study, a commercial pozzolan-based slurry is considered as a barrier material for primary cementing. It is a non-OPC material and it is primarily used as spacer fluid ahead of cement. Its rheological properties can be adjusted to the desired level and the slurry can set and develop strength at downhole conditions. No detailed information is available for the composition of this slurry. This material is used in the North Sea. Therefore, test results of this material are added for benchmarking its performance.

1.3. Geopolymer

Inorganic polymers, known as geopolymer, are a class of cementitious materials produced by mixing a liquid hardener with reactive aluminosilicate species (Davidovits, 2013). The tetrahedral long-chain molecules that consist of aluminum and silicate are formed during geopolymerization reaction and hence, no hydration takes place. The solid phase that is broadly known as geopolymeric precursor, may include low calcium fly ash, thermally activated clay (metakaolin) or naturally occurring rocks (Khalifeh et al., 2019; Liu et al., 2020; Salehi et al., 2019). The liquid phase is an alkali (normally sodium or potassium) silicate solution with an optimum modular ratio. The reaction is known as geopolymerization and it consists of three main mechanisms: the dissolution of aluminosilicate structure of the solid phase in presence of hydroxyls and creation of silanol groups (Si–O–H), orientation and reconnection of molecules due to an increase in the concentration of ions in the slurry and forming oligomers and finally, polycondensation by connecting oligomers and forming a long-chain structure of aluminosilicates.

The geopolymers are already used in civil industry, but the technology is still under development for oil and gas applications by adjusting the rheological and mechanical properties in accordance with downhole conditions. Previous research works confirmed that rheological behavior and mechanical properties of geopolymers are temperature-dependent (Khalifeh et al., 2018; Paiva et al., 2018). In the current work, a naturally occurring rock normalized with other aluminosilicate sources (Alvi et al., 2020) is mixed with potassium silicate solution to produce the rock-based geopolymers.

1.4. Thermosetting resin

Organic thermally activated resins, broadly known as thermosetting resin, can be solidified when exposed to a predesigned temperature. Thermosetting resins are considered as particle-free liquid polymers and this feature allows penetrating micro fractures and seal the leak paths by forming heavy-molecule solids (Beharie et al., 2015; Cestari et al., 2009). Therefore, they are mainly used for remediation jobs to seal the micro crack or defected annular cement. Temperature, pressure and the composition of the liquid resin are the main variables in the polymerization reaction. Glass transition temperature in thermosetting resins is defined as the maximum temperature after which, the solid material enters into the plastic region and rigid behavior is not available no longer (Montserrat, 1993). Therefore, it is critical to have full control over the mix design of resin, operational condition, and geological temperature gradients in the drilling environment.

Thermosetting resins have been studied for potential P&A applications and in remedial field operations (Al-Ansari et al., 2015; Todorovic et al., 2016). This class of organic materials has shown interesting mechanical properties. The compressive strength is considerably higher than the OPC while they are more ductile. However, their volume shrinkage and exothermic reaction during solidification can introduce mechanical and thermal stresses at specific circumstances and bring concerns (Vrålstad et al., 2018). In this study, glass beads are used to adjust density of the slurry; hence, our system is not considered as particle-free system.

2. Test material preparation and experimental procedure

In all experiments, the slurries were mixed using the raw materials delivered by the industrial service providers and the mixing procedure was followed in accordance with the provided instructions. The mixing procedure for each cementitious material is described as follows:

Neat class G cement – The neat API class G cement manufactured by Dyckerhoff was mixed with 44% deionized water. API high-speed mixer, Waring blender, was used to mix the slurry.

Expansive cement – The dry blended API class G cement (Dyckerhoff) with magnesium oxide as an expansive agent was delivered by the material supplier. Industrial chemicals were added to the slurry to tailor the rheological and mechanical properties of the slurry. The additives included in this study were retarders, fluid-loss controller, defoamer and cement particle dispersant. Microsilica solution with a mass fraction of 50% in water was recommended by the cement supplier to enhance performance of the material.

Pozzolanic slurry – Common industrial chemicals that usually are used for controlling cement properties were applied to mix the slurry. A chemical activator was introduced to the slurry before pre-conditioning. The pozzolanic slurry was mixed and delivered by the material supplier.

Geopolymer – The precursor was dry blended in accordance with the recommended procedure. The solid phase was an aluminosilicate rich naturally occurring rock normalized by adding active quenched blast furnace slag (BFS), which is an industrial waste, to achieve normalized chemical composition. Potassium silicate solution with a modular ratio of 2.49 was used as hardener and mixed with solid phase before pre-conditioning. API high-speed model, Waring mixer, was used to mix the slurry.

Thermosetting resin – The liquid pre-mixed resin based of vinyl toluene was provided by the material supplier. Glass beads were used to increase the mass density of the resin mixture and a viscosifier was added to control the rheological properties. The slurry was mixed at 600 RPM using Heidolph overhead stirrer model Heigh-TORQUE. The materials used in this study are summarized in Table 1.

Slurry preparation – All the laboratory experiments performed in a specific condition of pressure and temperature to simulate downhole conditions; where the bottom-hole circulating temperature (BHCT) and bottom-hole static temperature (BHST) were selected to be 65 and 90 °C, respectively. The downhole pressure is considered to be 172 bar. For all laboratory experiments, the mixed slurries were pre-conditioned for 30 min at the BHCT, in accordance with API 10B-2 (American Petroleum

Table 1
Mix design of the of candidate barrier materials used in this study.

	Solid phase				Liquid phase by weight of solid (BWS)				Additives (BWS)			
	Class G	Naturally occurring rock	Glass bead	Deionized water	Potassium silicate solution	Pre-mixed resin	Micro silica solution (50%)	Fluid-loss controller	Cement dispersant	Defoamer	Cement retarder	Viscosifier
Neat class G	790			44%								
Expansive cement	790			33%			11%	2.8%	0.5%	0.1%	0.6%	
Pozzolanic material	No information available.											
Geopolymer		700			44.5%							
Thermosetting resin			720			50%						1%

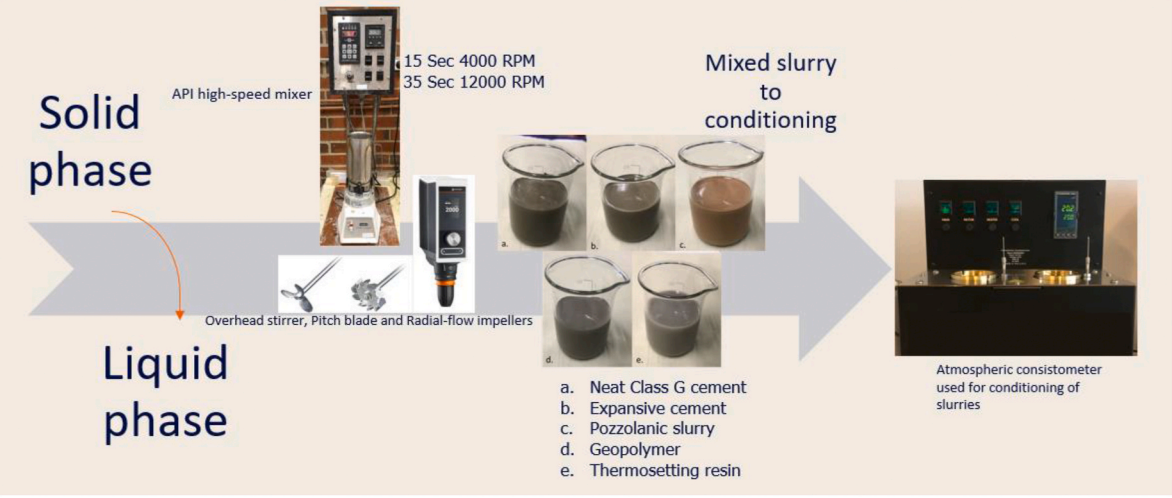

Fig. 2. Slurry sample preparation for laboratory tests.

Institute, 2013). The temperature ramp-up rate was 1 °C/min; after reaching the BHCT, the slurries were pre-conditioned for 30 min. Atmospheric consistometer, OFITE Model 60, was used for pre-conditioning of the slurries.

In Fig. 2, the slurry preparation up to conditioning before running laboratory experiments is shown graphically.

Viscosity measurement – Fann 35 rotational viscometer with configuration of R1-B1 was used for measuring the viscosity profiles. The viscometer cup was pre-heated to 65 °C for avoiding any thermal shock to the slurries. The test was performed following the API 10B-2 Recommended Practice (American Petroleum Institute, 2013). The average between the ramp-up and ramp down flow curves were used to calculate the viscosities at the different shear rates.

Static fluid-loss – The pre-conditioned slurries were transferred to the static fluid-loss test cell for measuring the performance of the slurries. The sampled fluid was measured at different time intervals, up to 30 min. For those slurries that experience break-through before 30 min, the following expression is used to report the API fluid-loss:

$$Fluid-loss = 2V_t\sqrt{\frac{30}{t}} \quad (1)$$

where V_t is total volume of the filtered liquid at the time of break-through, and t is the time in minute when the break-through occurs.

Pumpability – After loading the slurries in the relevant equipment, the temperature ramp-up rate was set equal to 1 °C/min until it reached to the BHCT and then the temperature was kept constant. Additionally, the consistency of the samples was measured at the elevated pressure of 172 bar with the pressure ramp-up of 17.2 bar/min. The equipment for measuring the consistency was OFITE Model 60 for atmospheric pressure and OFITE Model 2040 for elevated pressure. Both equipment sheared the slurries at 150 RPM; however, the paddles are different.

Uniaxial compressive strength (UCS) – The uniaxial compressive strength test was performed on samples cured at downhole condition of pressure and temperature after desired period of time. For UCS test, the specimens can be cured either in cubic forms with dimension of 50.8 mm (American Petroleum Institute, 2013) or in cylindrical mold with height to diameter (slenderness ratio) of 2.0 (American Petroleum Institute, 2017). The procedures for compressive strength test, and also non-destructive sonic strength development are described in API 10B-2. However, the test results only can be used to ensure that the cement has sufficient strength to resume drilling operation and they are not practically appropriate for annular cement integrity simulations (American Petroleum Institute, 2017). Hence, in this study, cylindrical specimens were considered to measure uniaxial compressive strength of the

materials. Two main reasonings for selecting cylindrical geometry are as following: a) the UCS test results can be more practical for cement sheath integrity simulations (American Petroleum Institute, 2017), b) practical issues such as design of the HPHT autoclave chambers used in this study.

Poly propylene plastic containers manufactured by VWR with diameter of 50 mm and height of 102 mm (see Fig. 4a) were used as mold. The molds can withstand the maximum temperature of 121 °C; therefore, they were applicable for curing the samples at 90 °C and under elevated pressure of 172 bar. After conditioning at BHCT, the slurries were poured in the molds and placed in the autoclaves for curing. Three samples were considered for each material and placed in the oven for different time intervals, 1-, 5-, 7- and 28-day (12 samples in total). Afterward, the hardened samples were removed from oven and gradually cooled down to ambient condition. Later, the samples were detached from the molds and both ends were flattened by using a cutting machine to eliminate the end effect during loading process (see Fig. 4b). Flattening both ends caused reduction in slenderness ratio below 2 that can overestimate the compressive strength of the barrier materials. Hence, the API 10TR7 for testing mechanical behavior of cement recommended correction factor that should be applied to each testing sample. For specimens with (l/d) < 2, API has referred to American Society for Testing and Materials, ASTM (2014) and correction factors can be either interpolating the range provided by Table 2, or using the polynomial equation in Fig. 3.

American Petroleum Institute (2017) recommends the constant compression stress rate in the range of 3.5 MPa/min to 14 MPa/min. However, due to technical limitations, the stress rate was selected equal to 35 MPa/min. According to a Cooperative Testing Results presented in Annex A, American Petroleum Institute (2017), the loading rate of 35 MPa/min results in lower compressive strength by 6% comparing to the loading rate of 14 MPa/min for the cylindrical specimens (American Petroleum Institute (2017)). The UCS machine used to conduct the tests was Toni Technik-H mechanical tester (see Fig. 4c).

Indirect tensile strength (Brazilian) – The same procedure as the UCS test was followed to cure the samples. Then, the cured samples were cut into the disc shapes with a thickness of about 30 mm and placed vertically between the curved jaws as shown in Fig. 4d. Zwick/Roell Z050 static material testing machine with a compression loading rate of 3 kN/min was employed to run the experiments (American Society for Testing and Materials, ASTM, 2016) and the tensile strength was calculated by the following equation.

$$\text{Tensile strength} = 1.2\frac{F}{\pi DL} \tag{2}$$

where F is the maximum tensile force, D is the diameter, and L is the thickness of the sample.

Sonic strength development – The pre-conditioned slurries were transferred to the ultrasonic cement analyzer (UCA) machine. The operational condition of temperature and pressure for the equipment was defined to be 90 °C and 172 bar, respectively. The temperature and pressure ramp-up rates were 1 °C/min and 17.2 bar/min. Chandler UCA Model 4265-HT was employed for this test. The machine is calibrated to test OPC, while for new materials, a novel algorithm must be provided and applied in the custom algorithm option.

Table 2
Correction factor of uniaxial compressive strength for specimens that have slenderness ratio below 2.

l/d	2	1.75	1.5	1.25	1
Correction factor	1	0.98	0.96	0.93	0.87

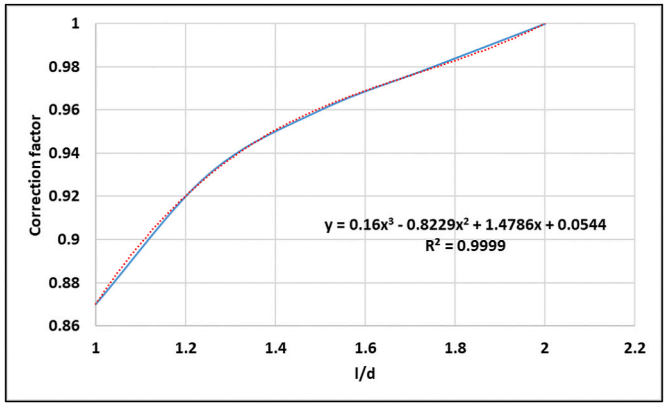

Fig. 3. Calculated correction factor by applying the polynomial equation for specimens with slenderness ratio less than 2.

3. Results and discussions

3.1. Rheological behavior and viscosity measurement

In this study, the viscosity of slurries was measured by the means of rotational viscometer. Fluid viscosity along with wellbore geometry (e.g. hole size, inclination and eccentricity) determines the frictional pressure losses and fluid displacement quality in the wellbore. Hence, accurate viscosity measurement and data fitted to an appropriate model are necessary. Among several suggested models for the drilling fluids, Herschel – Bulkley model is the simplest three-parameter model to describe the viscosity of non-Newtonian fluids over a range of shear rates (Herschel and Bulkley, 1926). In this model, shear stress (τ) at any shear rate ($\dot{\gamma}$) is presented as:

$$\tau = \tau_y + K\dot{\gamma}^n, \tau > \tau_y \tag{3}$$

$$\dot{\gamma} = 0 \quad \tau \leq \tau_y$$

where τ_y is the yield stress and n is the flow index, both are unique values and depending on the composition of the slurry. K is consistency factor and depends on the flow index. Hence, K cannot represent the properties of the fluid in fluid comparisons. Consequently, considering the Herschel – Bulkley approach and modelling the fluid behavior by curve fitting method may result in various combinations of K and n for the same data set. Saasen and Ytrehus (2018) re-arranged the Herschel – Bulkley model based on the suggested approach by Nelson and Ewoldt (2017) and introduced a surplus shear stress, τ_s and surplus shea rate, $\dot{\gamma}_s$, both are unique parameters for each fluid and the flow situation. The new model is defined as follows:

$$\tau = \tau_y + \tau_s\left(\frac{\dot{\gamma}}{\dot{\gamma}_s}\right)^n, \tag{4}$$

where $\tau_s = \tau - \tau_y$ at. $\dot{\gamma} = \dot{\gamma}_s$

The equation suggested by Power and Zamora (2003) provides an acceptable approximation for the yield stress:

$$\tau_y = 2\tau_3 - \tau_6 \tag{5}$$

The next step is to determine the surplus shear rate and the related surplus shear stress. Geometry of flow path is one of the effective parameters in shear rates. In primary cementing operation, the cement slurry flows in a pipe or in the annular area behind casing. Moreover, the flowrate at which the cement slurry is pumped can influence the shear rate. Usually, the shear rate of 102.2 s^{-1} (the pumping flow rate of about 1300 L/min in 9 5/8-in. to 12 ¼-in. annulus) is typical in cementing operations. This shear rate is equal to 60 RPM in bob and cylinder rotational viscometer. Subsequently, to determine the curvature

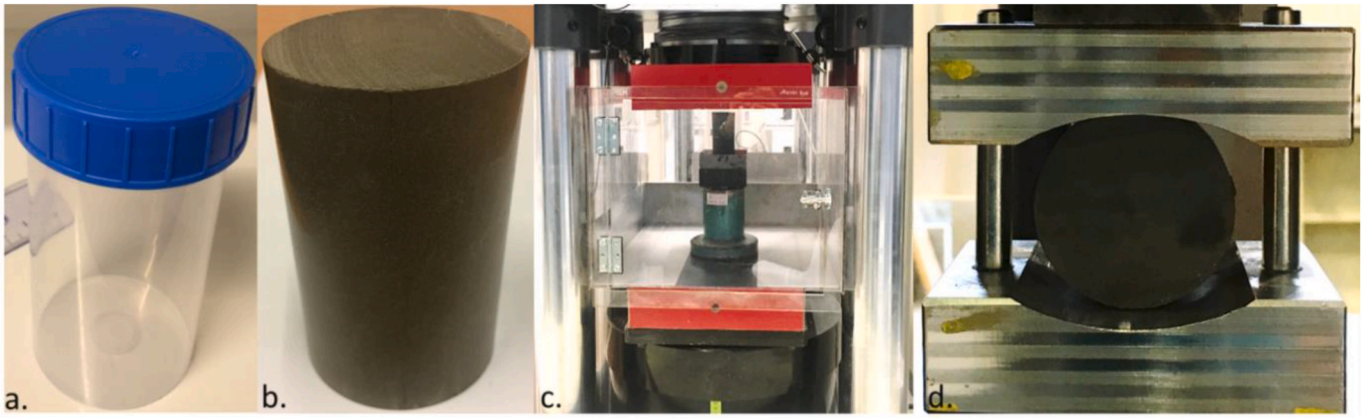

Fig. 4. a) The plastic mold used for curing the samples, b) Cured sample after flattened both ends, c) UCS test setup, d) Indirect tensile strength test setup.

Table 3
Density, pH, viscosity model parameters, fluid loss and consistency of the materials.

	Density (sg.)	pH	Gel Strength (Pa)		Viscosity model parameters				API Fluid Loss (ml)	Pumpability (min)	
			10-sec	10-min	ty	τ_s	n_{ls}	n_{hs}		ATM	PRS
Neat class G	1.9	13.6	11.75	69.5	6.13	31.68	0.98	0.29	821.04	132	96
Expansive cement	1.95	13.2	12.2	40.3	7.4	44.2	0.64	0.65	21	462.5	338.5
Pozzolanic material	1.68	13.3	3.57	5.11	2.04	26.65	0.72	0.70	18.8	N/A	N/A
Geopolymer	1.95	13.4	12.2	23	7.78	28.11	0.95	0.87	0	120	110
Thermosetting resin	1.65	N/A	3.5	19.4	3.32	38.58	0.844	0.82	183.76	293	263.5

N/A: Not Applicable

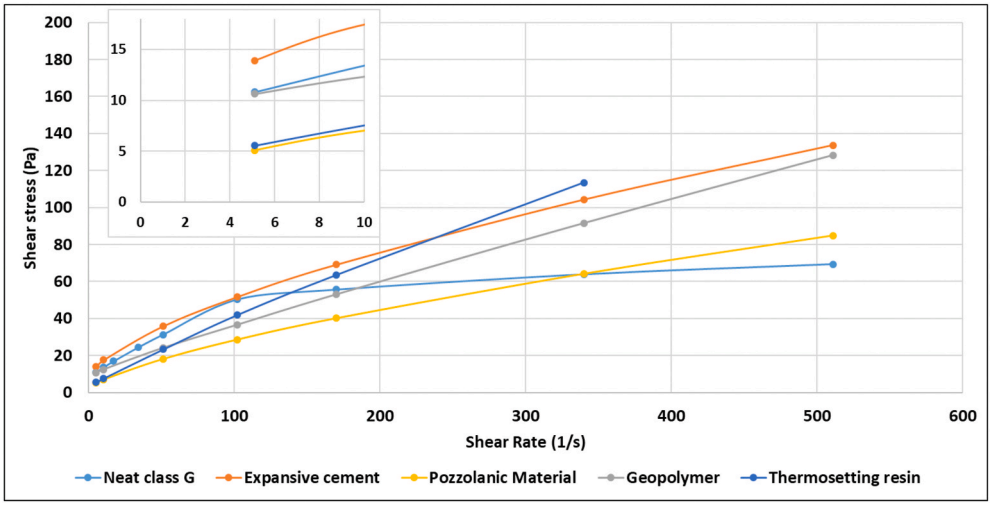

Fig. 5. Viscosity profile of the candidate barrier materials at 65 °C.

component in the model. Two different values can be estimated, one at shear rates below and one for the shear rates above the surplus shear rate, aiming to increase the accuracy of the prediction and they are labelled as n_{ls} and n_{hs}. The mentioned parameters can be calculated at 30 and 200 RPM as follows, respectively:

$$n_{ls} = \frac{\ln\left(\frac{\tau_{30} - \tau_y}{\tau_s}\right)}{\ln\left(\frac{\gamma_{30}}{\gamma_s}\right)} \quad (6)$$

$$n_{hs} = \frac{\ln\left(\frac{\tau_{200} - \tau_y}{\tau_s}\right)}{\ln\left(\frac{\gamma_{200}}{\gamma_s}\right)} \quad (7)$$

For all materials, the 10-sec and 10-min static gel strengths were measured at constant temperature of 65 °C and they are summarized in Table 3.

The viscosity profile of the barrier materials at 65 °C and atmospheric pressure, right after pre-conditioning is presented in Fig. 5. As all the slurries have yield stress and a flow index less than unity, they are non-Newtonian with a shear thinning behavior. They are pumpable at typical operational pumping rates. The static gel strength test was performed after 10 s and 10 min at 3 RPM. All the fluids develop gel strength during a static period. The yield stress for the thermosetting resin and pozzolanic material was less than the other materials, but the viscosity of the resin was higher at higher shear rates, which the dial

reading at 300 RPM was not achieved. The glass beads that added to the system as the weighting agent can have an influence on the fluid behavior and make a plug flow at higher shear rates. The same procedure was followed for the neat class G cement, where the measured shear stress at 102 s^{-1} for the neat class G was unexpectedly high. A possible human or equipment error was suspected. However, repeating the tests three times confirmed the accuracy of the observation. The operational shear rate for cementing operation barely passes 200 s^{-1} and it means that there will be no concern about the placeability of the slurries (Nelson and Guillot, 2006).

3.2. Static fluid-loss test

The static fluid-loss was measured by API recommended apparatus. In primary cementing operation, during placement and post-placement before the material solidifies, the formation can act as a filter and hydrostatic pressure above the slurry can squeeze slurry filtrate into the formation. The loss of liquid phase can result in building particle bridges across the annulus and, hence, reducing in hydrostatic pressure in the annulus and increasing the risk of reservoir fluid invasion into the barrier sheath. Such liquid may also have a critical role in the setting process and maintaining the desired mechanical properties for the life cycle of the well. Moreover, fluid-loss can also negatively affect the rheological properties and consequently, placeability of the slurry all the way up behind the casing as it becomes thicker when the liquid phase leaves the mixture. From the operational point of view, the cement slurry should be placed at the predesigned depth and with the predefined pumping rate and without significant change in the composition. Increasing the pump pressure to place a thick slurry that already lost a part of its liquid can accelerate the fluid loss and fracture formation. However, in remedial operations, a high slurry loss (i.e. including the liquid phase and particles) value is a benefit for cement squeezing, when the fluid loss can result in cement bridge-off to seal the leak path. The guidelines for fluid loss control have been developed based on the field experiences, not the theoretical models. Hence, the operators have different specification about the acceptable fluid loss and the value may vary depending on the drilling environment and formation, but the values below 50 ml per 30 min are favourable for primary cementing (Bensted, 1998).

The result of static fluid-loss of the slurries after 30 min preconditioning at 65 °C is presented in Fig. 6. The geopolymer slurry revealed no fluid-loss during the testing time, which means that there is no free fluid and the geopolymeric species present in the slurry are well attached to the hardener phase. Although the hardener composition has a crucial effect on the test results, literature shows that modification of particle size of geopolymeric precursors reduces the fluid loss by 100% comparing to the previous tests performed by Khalifeh et al. (2019). The pozzolanic slurry and expansive cement indicated an acceptable result, approximately 10 ml after 30 min. This is mainly due to particle size distribution and fluid-loss control agents used in these mixtures. The thermosetting resin, however, experienced break-through just 8 min after running the test. Although the glass beads were used as weighting agent and the system is not particle-free, they were not able to bond to the liquid resin during the mixing and pre-conditioning. Consequently, extensive fluid-loss was experienced. The loss of water from the neat G cement was intensive and the break-through occurred only 3 min after running the test. The API static fluid-loss values for the thermosetting resin and class G cement reported in Table 3 show higher than that of the liquid phase added to mix the slurry. The physical meaning of these values can be described as if the slurry is connected to the source of the liquid phase, the tabulated value can be passed as filtrate in 30 min.

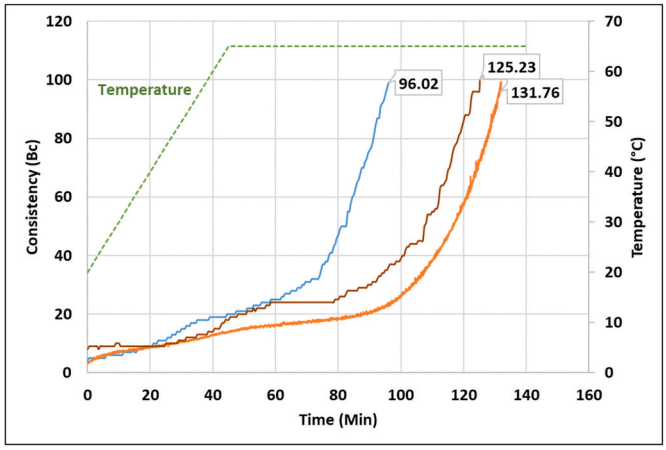

Fig. 7. The consistence of the neat class G cement slurry as function of time. Orange curve: Atmospheric consistometer. Brown curve: Pressurised consistometer at atmospheric conditions. Blue curve: Pressurised consistometer at elevated pressure. Numeric values are thickening time to 100 Bc (min). (For interpretation of the references to colour in this figure legend, the reader is referred to the Web version of this article.)

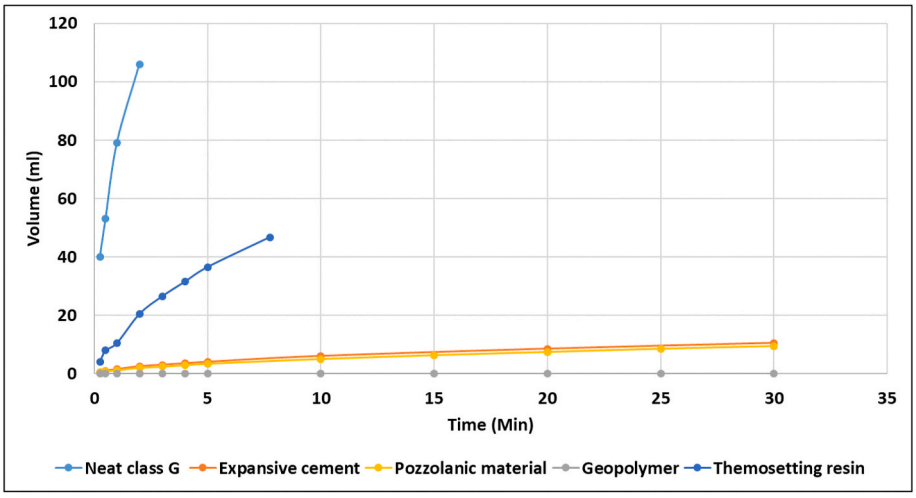

Fig. 6. Static fluid-loss of the barrier materials.

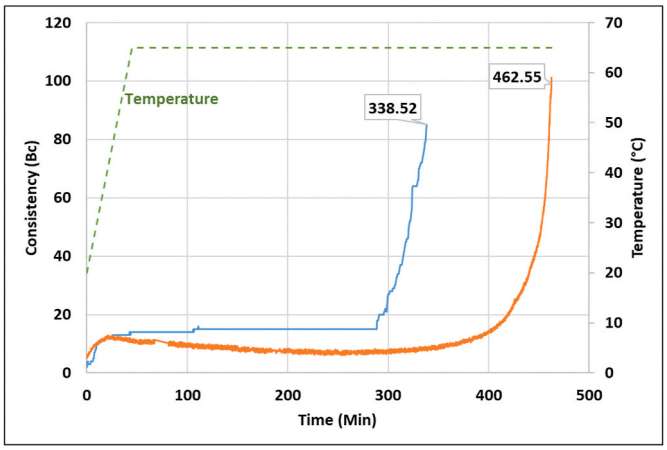

Fig. 8. The consistence of the expansive cement slurry as function of time. Orange curve: Atmospheric consistometer. Blue curve: Pressurised consistometer at elevated pressure. Numeric values are thickening time to 100 Bc (min). (For interpretation of the references to colour in this figure legend, the reader is referred to the Web version of this article.)

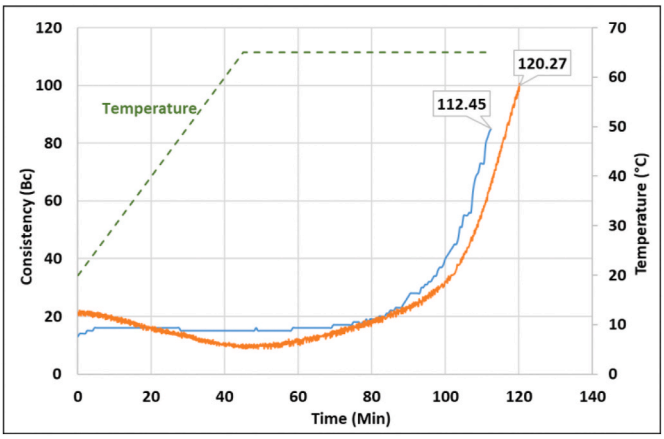

Fig. 10. The consistence of the geopolymer slurry as function of time. Orange curve: Atmospheric consistometer. Blue curve: Pressurised consistometer at elevated pressure. Numeric values are thickening time to 100 Bc (min). (For interpretation of the references to colour in this figure legend, the reader is referred to the Web version of this article.)

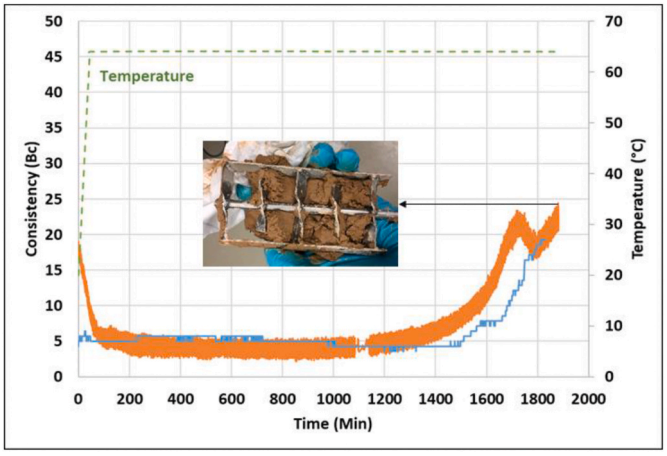

Fig. 9. The consistence of the pozzolanic material as function of time. Orange curve: Atmospheric consistometer. Blue curve: Pressurised consistometer at elevated pressure. (For interpretation of the references to colour in this figure legend, the reader is referred to the Web version of this article.)

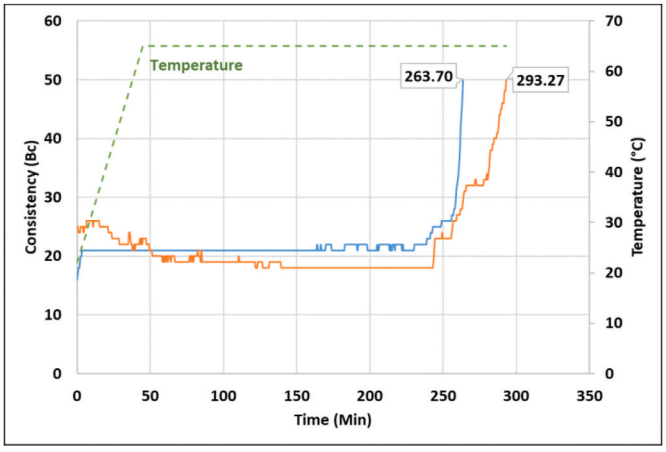

Fig. 11. The consistence of the thermosetting resin slurry as function of time. Orange curve: Atmospheric consistometer. Blue curve: Pressurised consistometer at elevated pressure. Numeric values are thickening time to 100 Bc (min). (For interpretation of the references to colour in this figure legend, the reader is referred to the Web version of this article.)

3.3. Pumpability and consistency

The pumpability of the cementitious slurries was measured by measuring the torque of spring connected to a paddle. The paddle stirred the slurry continuously. Considering the consistency of setting materials, one should differentiate between pumping time and setting. Setting time is the time required for the material to set from gel status. Pumping time, also known as workability, is a property of setting material indicating how long the slurry remains in the fluid phase before gelation occurs. The test is usually performed at the BHCT and the instrument measures the consistency of the slurry in Bearden units of consistency (Bc). Depending on the operator's criteria, the upper limit for the pumpability varies between 30 and 40 Bc and beyond that, the cement mixture is considered as unpumpable or risky fluid because the slurry becomes thick. However, it is recommended to continue the test until it reaches 100 Bc (American Petroleum Institute, 2013). The reason is that the trend of the curve from 40 Bc to 100 Bc can provide an estimation about the strength of gel so that gas should not be able to attack the slurry before it sets. A rapid increase in the consistency during this period is known as Right-Angle Set, where the transition from liquid to the solid phase happens quickly and it can significantly reduce the risk of formation fluid invasion into the cement sheath, especially in gas wells or oil wells with shallow gas. However, it may increase the risk of setting in drill string or setting at undesired depth before reaching the end station.

The consistency of the candidate barrier materials at atmospheric and elevated pressure of 172 bar is shown in Figs. 7–11. As two different

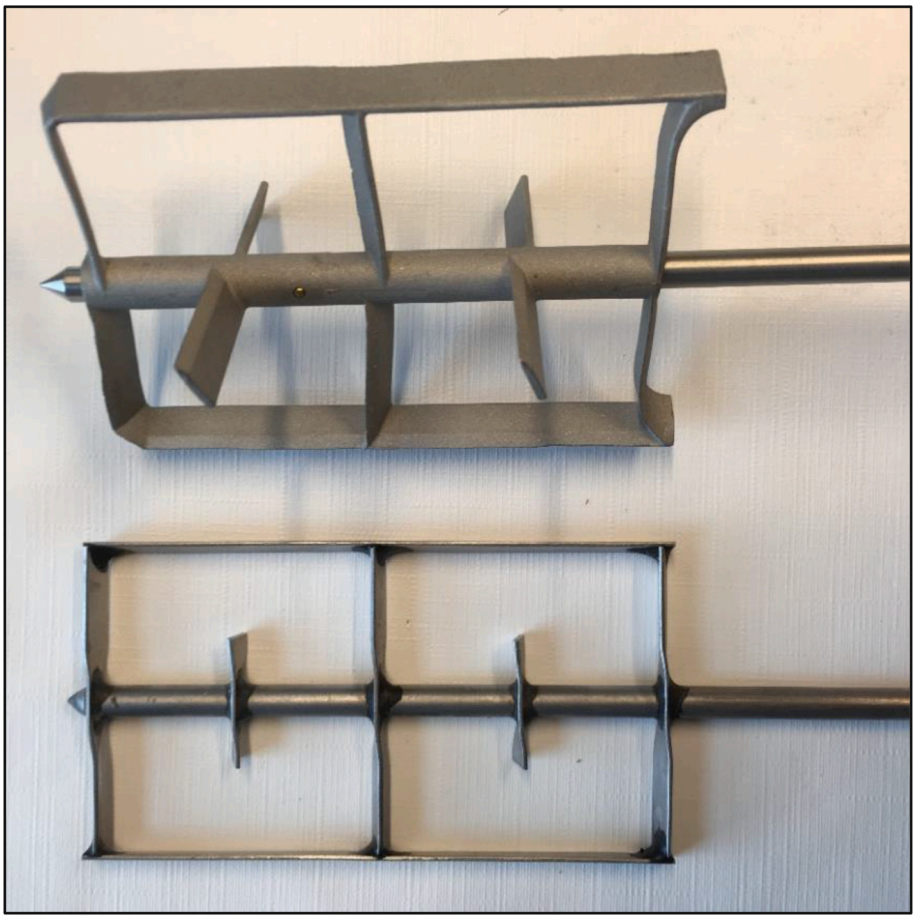

Fig. 12. The paddles that is used for shearing the mixed slurries in pressurised consistometer (upper device) and atmospheric consistometer (bottom device).

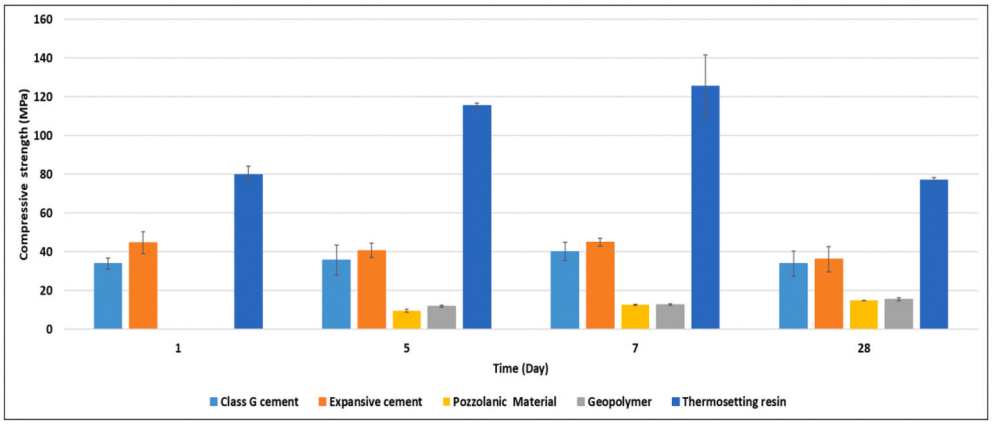

Fig. 13. Average compressive strength of the candidate barrier materials.

equipment were used to run the test at atmospheric and elevated pressure, an extra test was performed on the neat class G cement with the pressurised consistometer while the pressure was set at atmospheric level (brown curve). The reason was to test the reliability of the atmospheric consistometer and validity of the measurements. No significant difference was observed in the results; hence, the tests at atmospheric pressure were performed with atmospheric consistometer.

Increasing the pressure from atmospheric to 172 bar has an acceleration effect on the pumpability of all materiel to a different extent. For the neat class G cement, the acceleration effect was about 35 min which is about a 25% reduction in pumping time, while for the expansive cement the impact was slightly more pronounced. The expansive cement was pumpable for almost 7 h at atmospheric pressure and increasing the pressure reduced the pumpability to 5 h giving nearly a 26% reduction in pumping time. The kinetic of the governing chemical reactions and hydration of the components that exist in the chemical

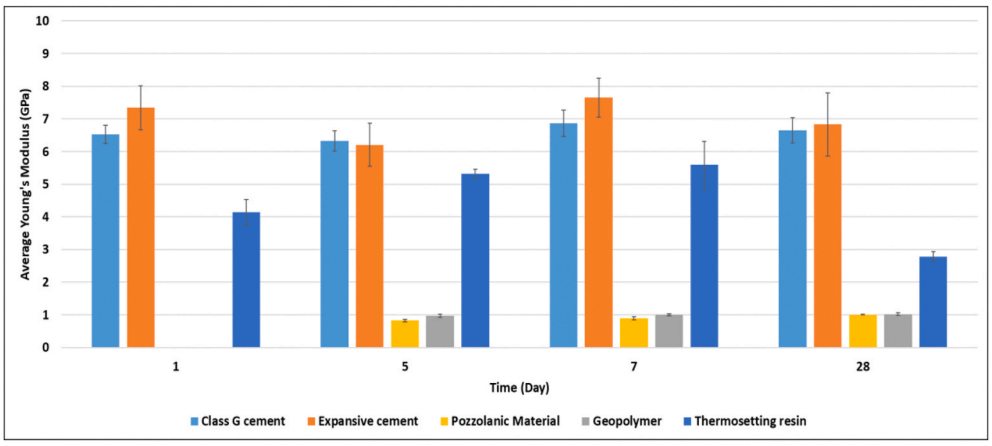

Fig. 14. Average Young's modulus of the barrier materials.

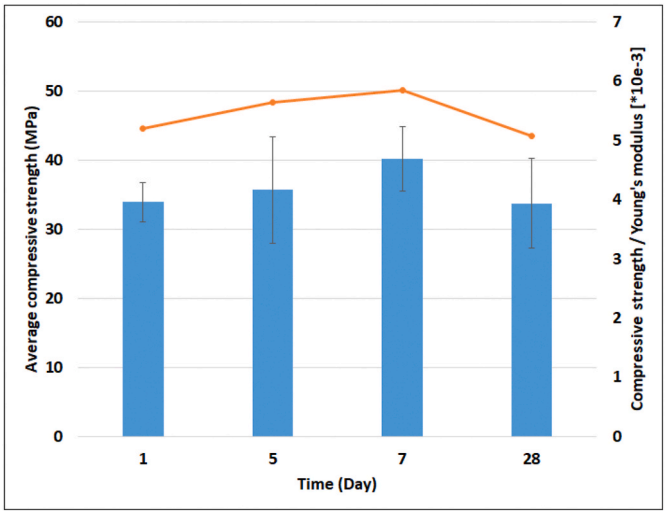

Fig. 15. Average uniaxial compressive strength (blue bars) and the compressive strength divided by Young's modulus (orange line) for the neat class G cement. (For interpretation of the references to colour in this figure legend, the reader is referred to the Web version of this article.)

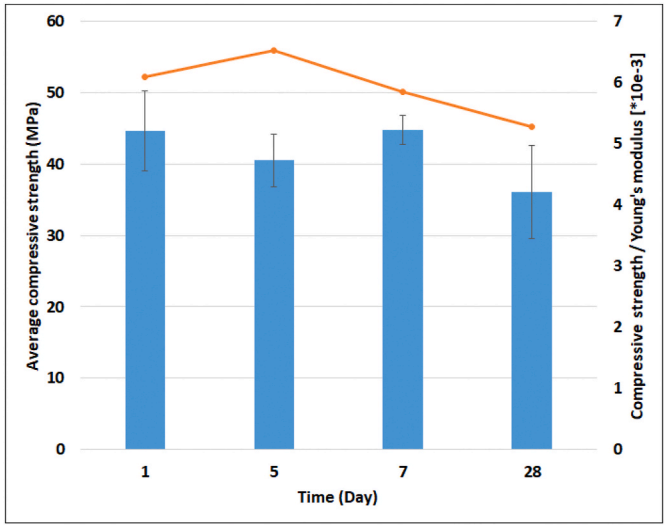

Fig. 16. Average uniaxial compressive strength (blue bars) and the compressive strength divided by Young's modulus (orange line) for the expansive cement. (For interpretation of the references to colour in this figure legend, the reader is referred to the Web version of this article.)

additives are likely pressure-sensitive (Wagh, 2016). These reactions have a significant influence on the formation of calcium-silicate-hydrate (C–S–H) gels and expedite gelation of the expansive cement. The consistency curve of the non-cement based pozzolanic slurry shows a constant trend up to 23 h after running the test. The curve reached a peak after 28 h and started to fluctuate. The test stopped at that stage and quick gelation happed only a few seconds after removing the sample from consistometers, Fig. 9. The test revealed how the static and dynamic condition affects gelation and setting time of the pozzolanic slurry. One may conclude that the physical damage to the gel structure of the material is the reason for having long thickening time. The geopolymer showed pressure independent pumpability. This has been confirmed by previous research conducted on the rock-based geopolymer (Khalifeh et al., 2019). Pumpability of the thermosetting resin was also pressure-dependent and it was reduced by 30 min by increasing the pressure, which is almost 10% reduction; however, the measured pumping time is still within the range recommended by operators. It might be valuable to study electrostatic forces between the particles or structure of solid phases for materials that showed pumping time-sensitive to pressure.

The expansive cement, geopolymer and thermosetting resin showed Right-Angle Set less than 15 min since the gelation phase started. Apart from the pressure as a variable in consistency tests, the effect of blade geometries of atmospheric and pressurised consistometers (see Fig. 12) is also recommended to be considered for future studies. The geometry of the paddle may affect the mixing energy or damaging the gel structures prior to the setting phase starts.

3.4. Uniaxial compressive strength (UCS) and flexibility

The average compressive strength of the barrier materials for the period of up to 28 days is presented in Fig. 13. The flexibility, compressive and tensile strength of the barrier material are linked together; increasing in ductility of the cementitious materials can result in a reduction of required compressive and tensile strengths (Jafariesfad et al., 2017a).

The average Young's modulus of each barrier material after curing the samples up to 28 days is shown in Fig. 14. The pozzolanic slurry and geopolymer were not able to develop early strength after 24 h curing under the bottom-hole condition. However, Young's modulus of these

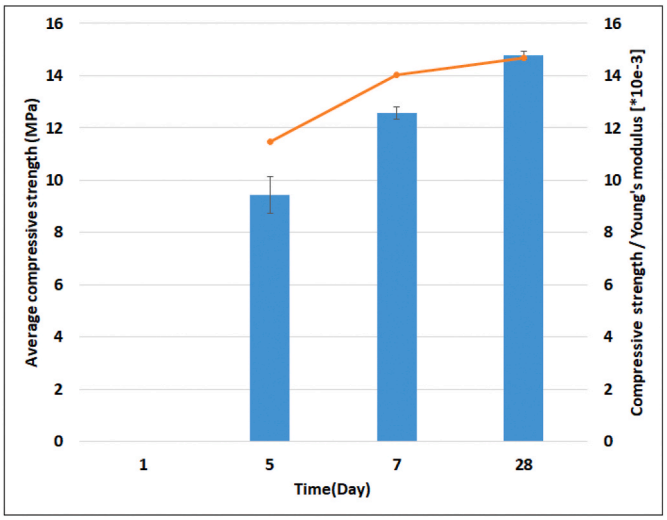

Fig. 17. Average uniaxial compressive strength (blue bars) and the compressive strength divided by Young's modulus (orange line) for the pozzolanic material. (For interpretation of the references to colour in this figure legend, the reader is referred to the Web version of this article.)

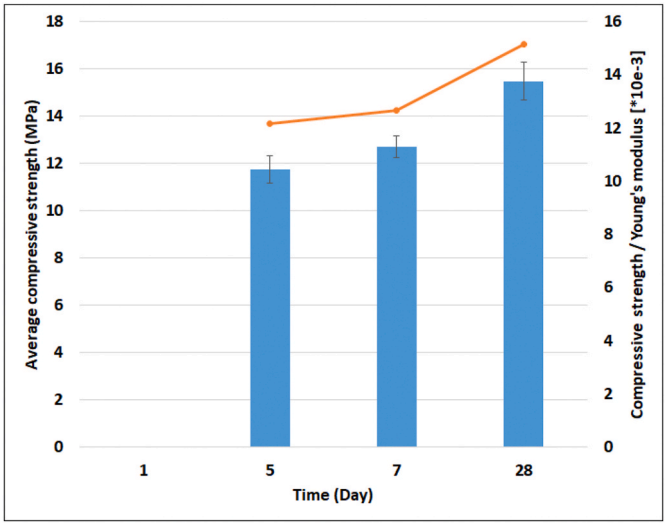

Fig. 18. Average uniaxial compressive strength (blue bars) and the compressive strength divided by Young's modulus (orange line) for the geopolymer. (For interpretation of the references to colour in this figure legend, the reader is referred to the Web version of this article.)

materials after 5, 7, and 28 days of curing were significantly low, and the materials were extremely flexible. Both the neat cement and the expandable cement systems showed constant flexibility during 28 days of curing. The modulus of flexibility for thermosetting resin was dropped by almost 50% after 28 days of curing.

In Figs. 15–19, the average uniaxial compressive strength (UCS) (right vertical axis) and the ratio of the UCS to Young's modulus (UCS/E) (left vertical axis) of the barrier materials are presented. The compressive strength of the neat class G cement has a slight decrease during the period from 7 to 28 days. This provides a motivation to investigate the change in the compressive strength for even longer periods. The compressive strength of the expansive cement was slightly decreased at the end of the testing period comparing to the results after 1-day curing and it became more ductile. After 28 days, the pozzolanic slurry and the geopolymer reached to the compressive strength of 14 and

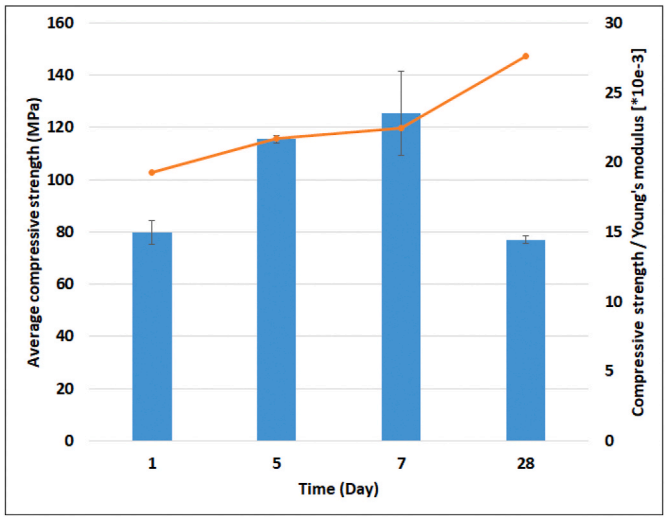

Fig. 19. Average uniaxial compressive strength (blue bars) and the compressive strength divided by Young's modulus (orange line) for the thermosetting resin. (For interpretation of the references to colour in this figure legend, the reader is referred to the Web version of this article.)

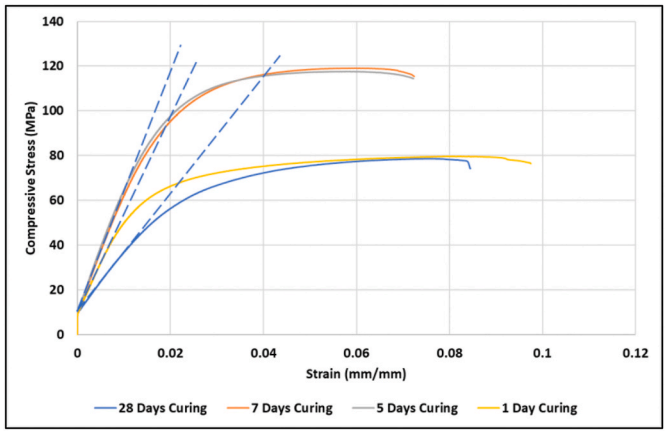

Fig. 20. Stress-strain curve for the thermosetting resin after curing at different time intervals.

16 MPa, respectively, and their trend for strength development was increasing for both materials. Although the thermosetting resins are not as brittle as cement, their UCS test was performed as described in the previous section to provide equal testing conditions for comparison with the other investigated materials. Perhaps development of standards for characterization of mechanical properties of thermosetting resin-based materials for utilization as zonal isolation materials is a necessity. The stress-stain curve for the material showed elastic behavior at earlier stage of the loading, almost similar to the other materials, but it enters to a plastic region. In other words, the plastic region in stress-strain curve of thermosetting resin was extended comparing to the other materials. However, the thermosetting resin was also cracked at failure point. Fig. 20 shows the stress-stain curve for the thermosetting resin.

The strength development trend for the thermosetting resin was reached to the maximum value of 130 MPa after 7 days; almost three times greater than the neat class G cement, but the value was dropped by almost 40% to 80 MPa after 28 days. Nevertheless, the UCS/E parameter increased due to the ductility of the material in this period. In Fig. 21 it is provided a comparison of the UCS/E value for all the five barrier materials for the testing period. The observations in results of UCS tests and

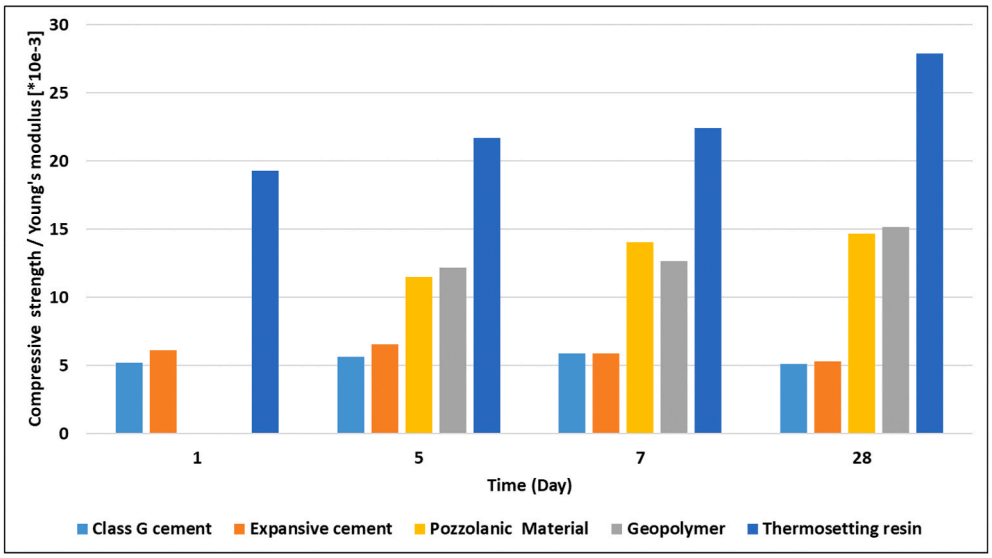

Fig. 21. The ratio of compressive strength to Young's modulus of the candidate barrier materials.

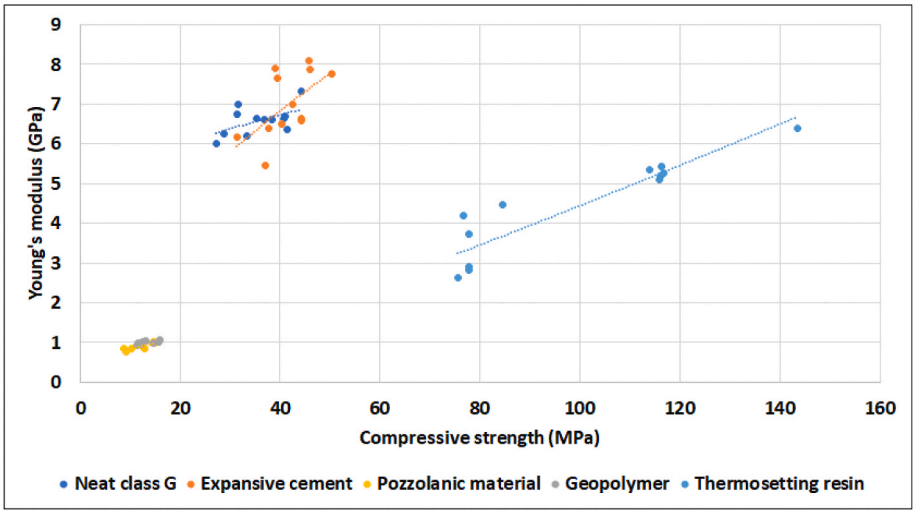

Fig. 22. Modulus of elasticity as function of compressive strength for five barrier materials.

Table 4
Young's modulus and compressive strength relationship equation parameters.

	Model parameters		Minimum WLS
	a	b	
Neat class G cement	2.560	0.2607	0.015
Expansive cement	0.701	0.6133	0.105
Pozzolanic material	0.732	0.1346	0.007
Geopolymer	0.544	0.2342	0.006
Thermosetting resin	0.015	1.2230	0.191

Table 5
Generated customised algorithm of the barrier materials for the UCA test based on data up to 28 days.

Material	Polynomial equation	R-square value
Class G cement	$y = 125.77x2 - 3701.1x + 226795$	0.9822
Expansive cement	$y = 190.85x^2 - 5281.6x + 35842$	0.9788
Pozzolanic material	$y = 365.82x^2 - 9880.6x + 65261$	0.9907
Geopolymer	$y = 28.662x^2 - 1310.9x + 12057$	0.995
Thermosetting resin	$y = 250.9x^2 - 9065.9x + 80945$	0.8502

the change in the ratio of UCS to Young's modulus have amplified the motivation to investigate the change in mechanical properties of all barrier materials in long-term. In addition, one needs to characterize the microstructure of these materials by the use of XRD and SEM techniques, to investigate any phase changes or transformation of the minerals.

3.4.1. Relationship between compressive strength and modulus of elasticity

Regularly the flexibility index is expressed in terms of compressive strength. Tomosawa and Noguchi (1993) analysed more than 3000 data of compressive strength for different types of heterogeneous concrete. They proposed a universal equation to estimate the structural deformation of concretes with compressive strength ranging between 20 and 160 MPa. The power-equation (Equation (8)) covers the compressive strength and mass density of the tested materials; besides, a correction factor takes into account the coarse aggregates and mineral admixtures in the concrete systems.

$$E = k_1.k_2.1486.\sigma_C^{\frac{1}{3}}.\gamma^2 \quad (8)$$

where E is the modulus of elasticity in MPa, k_1 and k_2 are the correction

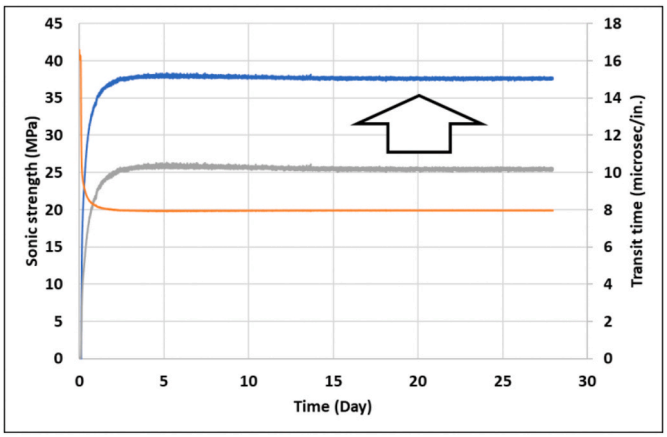

Fig. 23. Sonic strength development based on default algorithm of the equipment (grey line), Sonic strength development based on the generated algorithm (blue line) and the transit time (orange line) for the neat class G cement. (For interpretation of the references to colour in this figure legend, the reader is referred to the Web version of this article.)

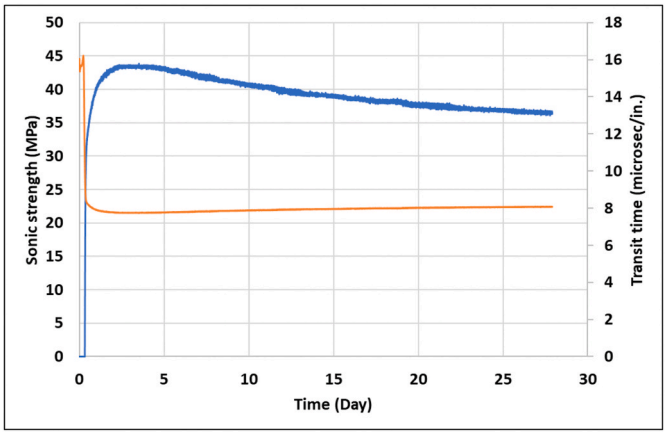

Fig. 24. Sonic strength development (blue line) and the transit time (orange line) for the expansive cement. (For interpretation of the references to colour in this figure legend, the reader is referred to the Web version of this article.)

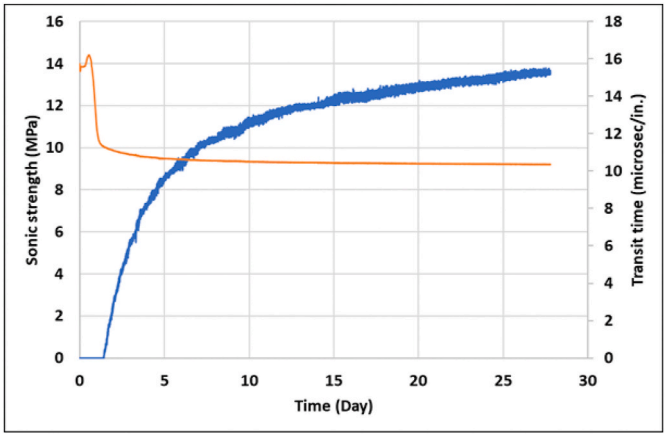

Fig. 25. Sonic strength development (blue line) and the transit time (orange line) for the pozzolanic material. (For interpretation of the references to colour in this figure legend, the reader is referred to the Web version of this article.)

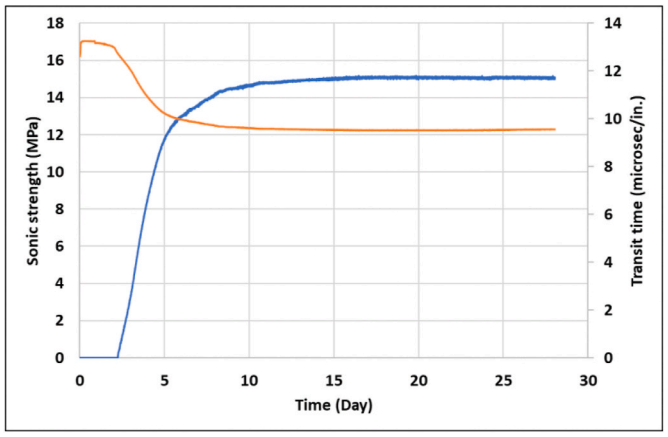

Fig. 26. Sonic strength development (blue line) and the transit time (orange line) for the geopolymer. (For interpretation of the references to colour in this figure legend, the reader is referred to the Web version of this article.)

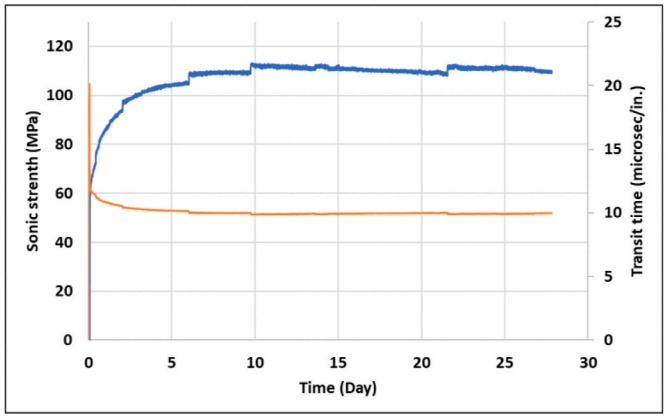

Fig. 27. Sonic strength development (blue line) and the transit time (orange line) for the thermosetting resin. (For interpretation of the references to colour in this figure legend, the reader is referred to the Web version of this article.)

factors defining the coarse aggregates and mineral admixtures, σ_C is the compressive strength in MPa, and γ is the mass density in Kg/l.

In this study, a regression analysis of over 12 crushed samples per each material was conducted based on the UCS test results, Fig. 22. Considering the universal equation suggested by Tomosawa and Noguchi (1993), a general equation was proposed to relate the short-term compressive strength of the materials as the explanatory variable and modulus of elasticity as the target variable. The suggested equations can predict the ductility of the materials with an acceptable accuracy at specific operational pressure and temperature in this project. All the slurries were mixed based on a fixed recipe; hence, the density of all materials is constant in the equation and can be neglected. Moreover, a homogeneous solid phase with constant mineralogy was used to mix and cure the barrier materials in entire tests. Consequently, the general equation can be simplified as a power function to the following form:

$$E = a.\sigma_C^b \quad (9)$$

In the equation above, the modulus of elasticity, E, is in GPa and σ_B is in MPa. Frequently, the least squares regression methodology is used to reduce the deviation between the model calculations and direct measurements. In this practice, the minimum weighted least squares (WLS) method is considered for finding the optimum values for a and b

constants in the general equation. The values for the constants are summarized in Table 4. The pozzolanic and geopolymeric materials showed the minimum WLS and it is an indication of homogeneity of the samples.

3.5. Sonic strength development

The ultrasonic cement analyser is able to estimate the strength development of the setting materials by measuring the sonic wave transit time through the slurries. Transit time of the sonic wave is a direct measurement by the equipment, and it is only dependent on the chemistry of the tested material. The software is programmed to convert the measured transit time to the compressive strength of the material based on a predefined algorithm introduced earlier to the system by the manufacturer. This algorithm is achieved based on previous experiments and it can provide a good estimation for the OPC. For setting materials other than OPC, the calculated compressive strength is not accurate, and a new algorithm should be introduced to the software. In this study, the UCS data were plotted versus the corresponding transit time measured by the equipment at the same period of curing time. Hence, four points were available for the neat class G, expansive cement and thermosetting resin while three points were available for the pozzolanic slurry and geopolymer. The generated algorithm for individual barrier material is presented in Table 5.

In Figs. 23–27, the sonic strength development (left vertical axis) and transit time (right vertical axis) for the candidate barrier materials are presented. The change in sonic strength development determined using the default algorithm for the neat class G cement is shown in Fig. 23. These values do not correspond with the crushing tests shown in Fig. 16. Hence, a new algorithm was made. The results from using this algorithm are shown by the blue curve in Fig. 23. The mechanical strength of the expansive cement started to decline 4 days after curing. A consecutive reaction corresponding to the chemical additives may cause a reduction in strength of the material. One possible scenario could be activation of the expansive agent that may create internal pressures. The trends of the pozzolanic material and geopolymer confirm that both materials had no strength up to 2 days after running the test, but the strength development was still ongoing after 28 days of the UCA test. The thermosetting resin was set fast at 90 °C and 2500 psi, but the corresponding plot shows a number of jumps in strength development trend. Coagulation of the weighting agents may be the reason for the sudden peaks in the trend; therefore, studying the non-zero zeta potential of the particles might explain the behavior of the material at this operational condition. Comparing the results from the UCA test with strength development in consistency curves can inform that how dynamic condition impacts the gelation of the materials, while its also essential to take into account the 25 °C difference in temperature in both tests, difference between BHST and BHCT. This effect on the thermosetting resin was intensive as static condition accelerates the gelation by 3 h. The dynamic condition effect was also observed for the pozzolanic material earlier in consistency test. A gap of 10-h is recognized between gelation and the strength development result of UCA test, which means that although the materials have formed gel after 28 h, it has not been set until about 40 h under 90 °C and static condition.

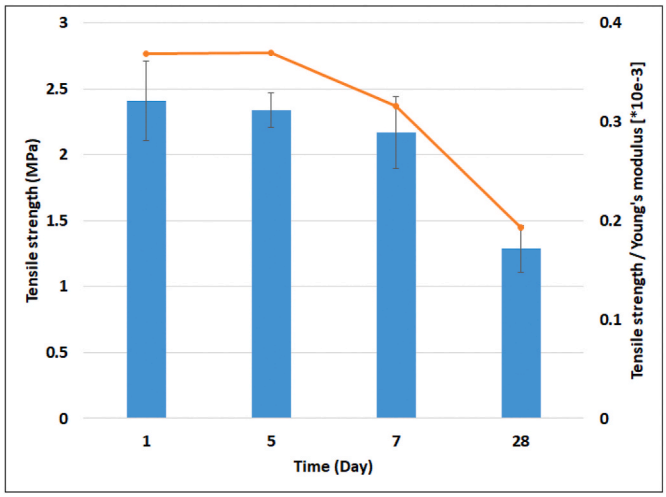

Fig. 29. Average tensile strength (blue bars) and the tensile strength divided by Young's modulus (orange line) for the neat class G cement. (For interpretation of the references to colour in this figure legend, the reader is referred to the Web version of this article.)

3.6. Indirect tensile strength (Brazilian) test

At downhole condition, the thermal and pressure loads occur during well completion and production period induce considerable tensions in complex directions to the cement sheath. These loads can arise well integrity challenges that may result in poor bonding of setting material to the casing/formation or the barriers with low tensile strength. The required tensile strength depends on the complex loadings on the barrier sheath as well as the mechanical properties of the nearby formation. Jafariesfad et al. (2017a) reviewed the typical loading modes and

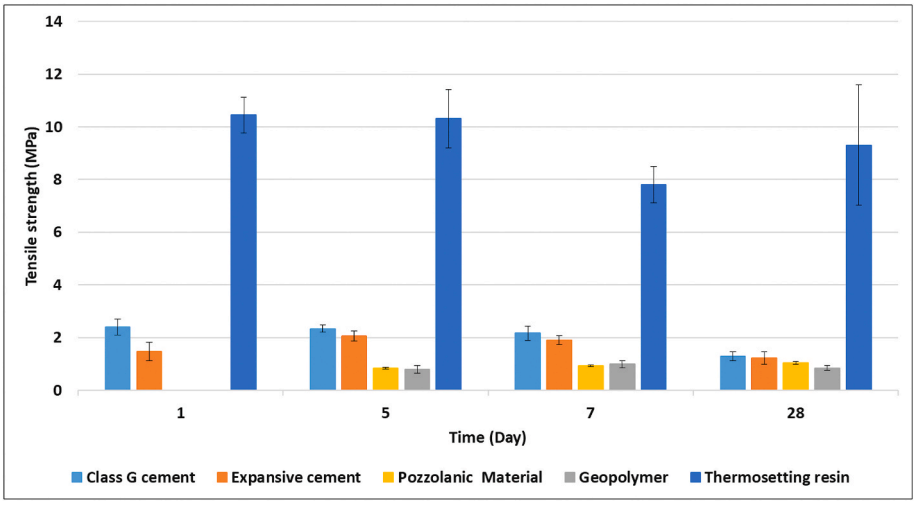

Fig. 28. Average tensile strength of the candidate barrier materials.

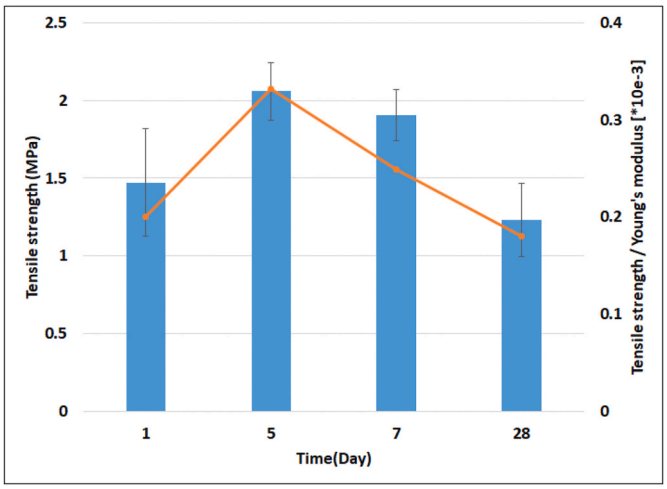

Fig. 30. Average tensile strength (blue bars) and the tensile strength divided by Young's modulus (orange line) for the expansive cement. (For interpretation of the references to colour in this figure legend, the reader is referred to the Web version of this article.)

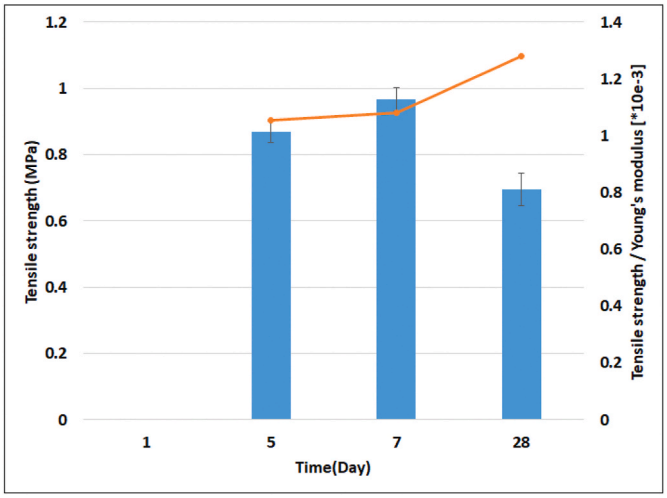

Fig. 31. Average tensile strength (blue bars) and the tensile strength divided by Young's modulus (orange line) for the pozzolanic material. (For interpretation of the references to colour in this figure legend, the reader is referred to the Web version of this article.)

minimum requirements to prevent the failure in barrier systems. They stated that for a different combination of radial and tangential stresses, Young's modulus affects the required tensile strengths to sustain zonal isolation and consequently, a higher ratio of tensile strength to Young's modulus is required.

In Fig. 28, it is shown the average tensile strength of the candidate barrier materials during a time span of 28 days. In Figs. 29–33, it is shown the average tensile strength (TS) (right vertical axis) and the ratio of tensile strength to Young's modulus (TS/E) (left vertical axis) of the barrier materials. All the candidate materials showed a decline in tensile strength between 7 days and 28 days of curing; except for the thermosetting resin, which experienced an increasing trend. The ratio of the tensile strength to Young's modulus of the cement system was declined after it reached a peak at 5 days. This parameter was almost constant for the pozzolanic material and geopolymer but for the thermosetting resin, it increased by more than 100% due to an increase in ductility and tensile strength. Fig. 34 provides a comparison of tensile strength over Young's modulus value for all five barrier materials for the testing period.

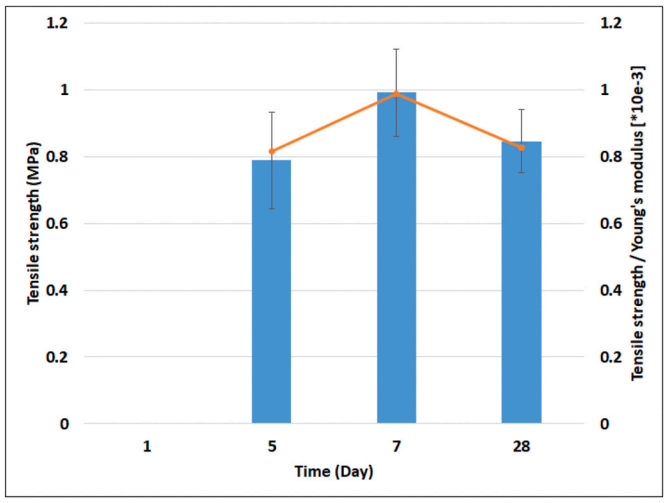

Fig. 32. Average tensile strength (blue bars) and the tensile strength divided by Young's modulus (orange line) for the geopolymer. (For interpretation of the references to colour in this figure legend, the reader is referred to the Web version of this article.)

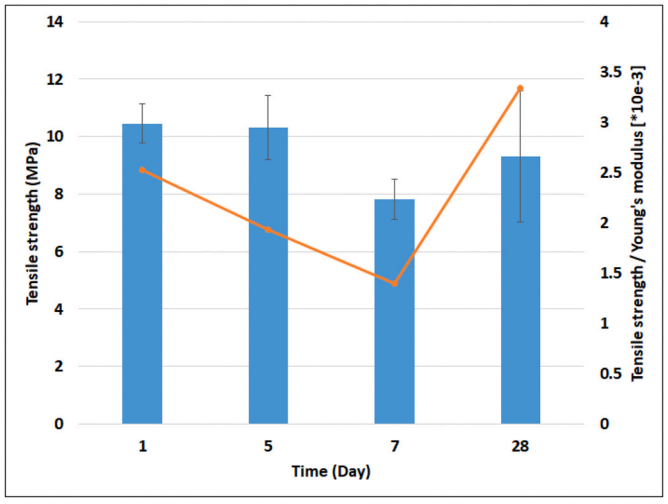

Fig. 33. Average tensile strength (blue bars) and the tensile strength divided by Young's modulus (orange line) for the thermosetting resin. (For interpretation of the references to colour in this figure legend, the reader is referred to the Web version of this article.)

In geomechanics, it is well-established that tensile strength and UCS is related (Nazir et al., 2013). Although direct measurement or laboratory tests of mechanical properties is the more reliable, estimations of USC/tensile strength based on available data can reduce the cost and save time. In this paper, a correlation between UCS and indirect tensile strength of the candidate barrier materials was investigated. The sample preparation for each test was followed the same procedure and both solid and liquid phases were homogeneous for each curing time. The average value of UCS and tensile strength was used to find the correlation.

The dispersion of average UCS and tensile strength tests results of the candidate barrier materials is shown in Fig. 35. The correlation coefficient was calculated for the mentioned parameters (see Table 6). The calculated correlation coefficients revealed that for the pozzolanic material, there is a strong positive relationship between the UCS and tensile strength. The coefficients for the expansive cement and neat class G cement indicated a fairly positive relation between the mentioned mechanical properties; but for the thermosetting resin, the value shows a

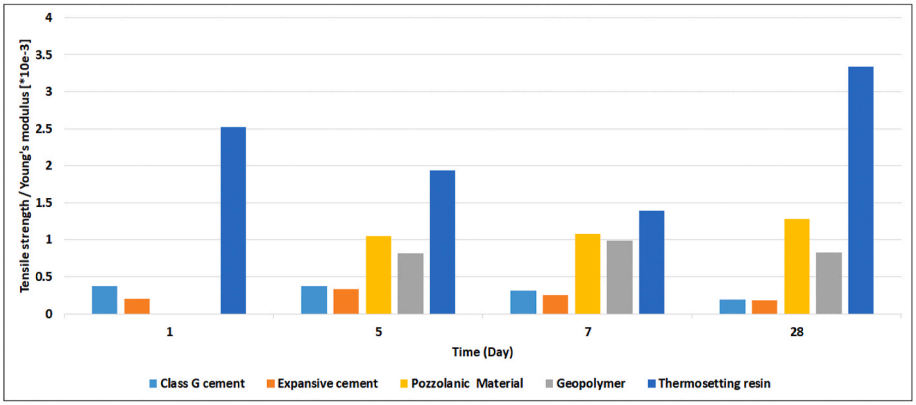

Fig. 34. The ratio of tensile strength to Young's modulus of the candidate barrier materials.

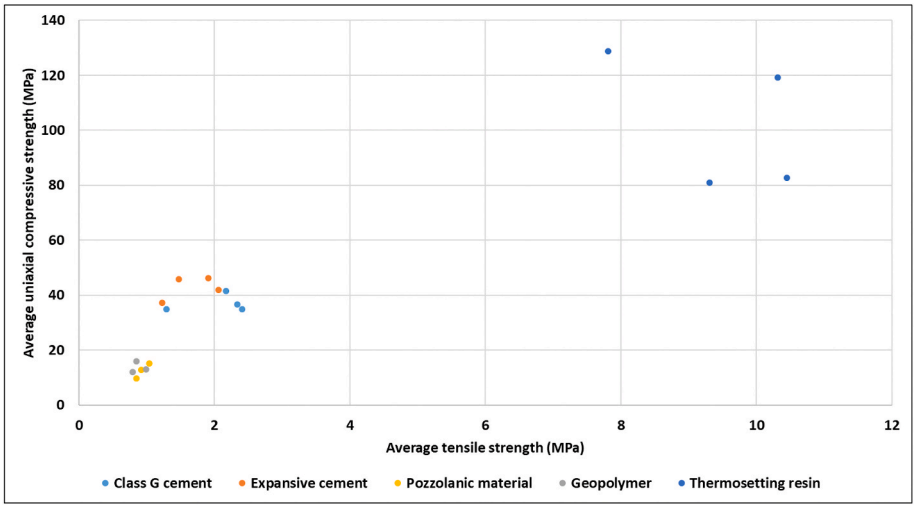

Fig. 35. Correlation between indirect tensile strength and UCS values for candidate barrier materials.

Table 6
Linear and power model parameters for the correlation between UCS and tensile strength of the barrier material.

	Power Model Parameters		Linear Model Parameters		Correlation coefficient	Power model Minimum WLS	Linear model Minimum WLS
	a	b	a	b			
Class G cement	33.52727	0.085083	1.52955	32.4155	0.294	0.016342	0.016744
Expansive cement	36.58101	0.234407	5.68501	31.58398	0.453	0.022118	0.023401
Pozzolanic material	13.9195	2.1149	28.14154	−14.1267	0.973	0.006746	0.005205
Geopolymer	13.2295	0.141667	1.812256	11.3871	−0.0003	0.03662	0.036794
Thermosetting resin	993.0011	−1.06013	−9.24029	179.9438	−0.5011	0.132749	0.141613

rather strong negative relationship. The calculated coefficient for the geopolymer was an indication of a weak relation between the UCS and tensile strength properties. Linear and power equations (Equation (10)) were considered to find an accurate relation between UCS and tensile strength and the minimum weighted least squares (WLS) method is considered for finding the optimum values for a and b constants in the general equation. The values for the constants are summarized in Table 6. The power model equation provides a better match based on available data, except for the pozzolanic material, which linear model fits better on the data set.

$$\sigma_C = a \times \sigma_T + b \quad \textit{Linear equation form}$$
$$\sigma_C = a \times \sigma_T^b \quad \textit{Power equation form} \tag{10}$$

4. Conclusions

Rheological and mechanical performance of five different zonal isolation materials were examined at equal operational condition of pressure and temperature. Albeit shortcomings of the neat API class G cement, it was selected as reference in this experimental project due to its well-known chemistry and properties. Thermosetting resin and pozzolanic material showed lower yield stress comparing to the geopolymer and cement systems; however, the pozzolanic material appear more shear-thinning compared to thermosetting resin. Expansive cement exhibits higher viscosity in majority of shear rates. The expansive cement, neat class G cement and thermosetting resins developed strong 10-min gel structure, but the geopolymeric and pozzolanic

slurries showed less time-dependent gel structure.

All the materials except the pozzolanic material showed right-angle set pumping profile. The pozzolanic material remained in liquid state while sheared in the consistometers. Expansive cement, neat G cement and thermosetting resin showed pressure-dependent performance. Static fluid-loss and pumpability of the materials showed acceptable values for the expansive cement, pozzolanic slurry and geopolymer, while the thermosetting resin experienced early breakthrough. The glass beads used as weighting agent were not able to bond to the liquid resin to perform as a fluid-loss controller.

Considering compressive strength development of the neat class G cement, expansive cement and thermosetting resin, a consecutive reaction takes in place which results in retrogression of the strengths. Early strength development of the pozzolanic and geopolymeric slurries is a concern as they did not develop strength up to two days of curing. Tensile strength of the thermosetting resin is 11% of its compressive strength cured for 28 days, but tensile strength of the other materials ranged 3.5–5% of their compressive strengths. Ductility of the neat class G and expansive cements, pozzolanic and geopolymer materials do not experience significant change during this testing period; however, the thermosetting resin becomes more ductile. Calculated compressive to Young's modulus and tensile strength to Young's modulus values showed that the thermosetting resins are more flexible with higher strength, followed by the geopolymeric and pozzolanic materials, and lastly the expansive cement and neat G cement.

Credit author statement

Mohammadreza Kamali: Conceptualization, Methodology, Investigation, Data curation, Writing – original draft, Writing – review & editing, Mahmoud Khalifeh: Conceptualization, Methodology, Writing – review & editing, Investigation, Resources, Supervision, Project administration, Funding acquisition, Arild Saasen: Conceptualization, Methodology, Writing – review & editing, Investigation, Resources, Supervision, Rune Godøy: Conceptualization, Methodology, Writing – review & editing, Investigation, Laurent Delabroy: Conceptualization, Methodology, Writing – review & editing, Investigation.

Declaration of competing interest

The authors declare that they have no known competing financial interests or personal relationships that could have appeared to influence the work reported in this paper.

Acknowledgement

The authors would like to thank the Ministry of Education and Integration in Norway for funding this project. Moreover, the authors gratefully acknowledge Halliburton, WellCem AS and AlTiSS AS for their supports and sharing technical information. A special thanks goes to Salim Taoutaou for sharing operational experiences. The authors thank Aker BP and TOTAL for supporting part of the project through the SafeRock Project joint industrial project at UiS.

References

Abid, K., Gholami, R., Tiong, M., Nagaratnam, B., Sarmadivaleh, M., Mostofi, M., Bing, C. H., Muktadir, G., 2019. A pozzolanic supplementary material to reinforce class G cement used for drilling and completion operations. J. Petrol. Sci. Eng. 177, 79–92.

Al-Ansari, A., Al-Refai, I., Al-Beshri, M., Pino, R., Leon, G., Knudsen, K., Sanabria, A., 2015. Thermal activated resin to avoid pressure build-up in casing-casing annulus (CCA). SPE Offshore Europe Conference and Exhibition. Society of Petroleum Engineers.

Al Ramadan, M., Salehi, S., Teodoriu, C., 2019. Robust Leakage Modeling for Plug and Abandonment Applications, International Conference on Offshore Mechanics and Arctic Engineering. American Society of Mechanical Engineers. V008T11A054.

Alvi, M.A.A., Khalifeh, M., Agonafir, M.B., August 2020. Effect of nanoparticles on properties of geopolymers designed for well cementing applications. J. Petrol. Sci. Eng. 191, 107128.

American Petroleum Institute, 2013. API RP 10B-2, Recommended Practice for Testing Well Cements. API, Washington, DC.

American Petroleum Institute, 2017. API TR 10TR7, Mechanical Behavior of Cement. API, Washington, DC.

American Society for Testing and Materials, ASTM, 2013. ASTM C311, Standard test methods for sampling and testing fly ash or natural pozzolans for use in portland-cement concrete. ASTM.

American Society for Testing and Materials, ASTM, 2014. ASTM-C39, Standard test method for compressive strength of cylindrical concrete specimens. ASTM.

American Society for Testing and Materials, ASTM, 2016. ASTM D3967-16, Standard Test Method for Splitting Tensile Strength of Intact Rock Core Specimens. American Society for Testing and Materials.

Baumgarte, C., Thiercelin, M., Klaus, D., 1999. Case studies of expanding cement to prevent microannular formation. SPE Annual Technical Conference and Exhibition. Society of Petroleum Engineers.

Beharie, C., Francis, S., Øvestad, K.H., 2015. Resin: an Alternative Barrier Solution Material, SPE Bergen One Day Seminar. Society of Petroleum Engineers.

Bensted, J., 1998. Special Cements, LEA's Chemistry of Cement and Concrete. Elsevier, pp. 783–840.

Cestari, A.R., Vieira, E.F., Tavares, A.M., Andrade Jr., M.A., 2009. An oilwell cement slurry additivated with bisphenol diglycidil ether/isophoronediamine—kinetic analysis and multivariate modelings at slurry/HCl interfaces. J. Hazard Mater. 170 (1), 374–381.

Davidovits, J., 2013. Geopolymer Cement. A Review, vol. 21. Geopolymer Institute, pp. 1–11. Technical papers.

Davies, R.J., Almond, S., Ward, R.S., Jackson, R.B., Adams, C., Worrall, F., Herringshaw, L.G., Gluyas, J.G., Whitehead, M.A., 2014. Oil and gas wells and their integrity: implications for shale and unconventional resource exploitation. Mar. Petrol. Geol. 56, 239–254.

Henkensiefken, R., Bentz, D., Nantung, T., Weiss, J., 2009. Volume change and cracking in internally cured mixtures made with saturated lightweight aggregate under sealed and unsealed conditions. Cement Concr. Compos. 31 (7), 427–437.

Herschel, W., Bulkley, R., 1926. Measurement of consistency as applied to rubber-benzene solutions. Am. Soc. Test Proc 621–633.

International Organization for Standardization, ISO, 2014. ISO/TS-16530, Well Integrity - part 1: Life Cycle Governance / Part 2: Well Integrity for Operational Phase. ISO.

Jafariesfad, N., Geiker, M.R., Gong, Y., Skalle, P., Zhang, Z., He, J., 2017a. Cement sheath modification using nanomaterials for long-term zonal isolation of oil wells. J. Petrol. Sci. Eng. 156, 662–672.

Jafariesfad, N., Geiker, M.R., Skalle, P., 2017b. Nanosized magnesium oxide with engineered expansive property for enhanced cement-system performance. SPE J. 22 (05): 1,681-1,689.

Jimenez, W.C., Urdaneta, J.A., Pang, X., Garzon, J.R., Nucci, G., Arias, H., 2016. Innovation of annular sealants during the past decades and their direct relationship with on/offshore wellbore economics. In: SPE Bergen One Day Seminar. Society of Petroleum Engineers.

Khalifeh, M., Saasen, A., Hodne, H., Godøy, R., Vrålstad, T., 2018. Geopolymers as an alternative for oil well cementing applications: a review of advantages and concerns. J. Energy Resour. Technol. 140 (9), 092801.

Khalifeh, M., Saasen, A., Hodne, H., Motra, H.B., 2019. Laboratory evaluation of rock-based geopolymers for zonal isolation and permanent P&A applications. J. Petrol. Sci. Eng. 175, 352–362.

Khalil, M., Amanda, A., Yunarti, R.T., Jan, B.M., Irawan, S., 2020. Synthesis and application of mesoporous silica nanoparticles as gas migration control additive in oil and gas cement. J. Petrol. Sci. Eng. 107660.

Kiran, R., Teodoriu, C., Dadmohammadi, Y., Nygaard, R., Wood, D., Mokhtari, M., Salehi, S., 2017. Identification and evaluation of well integrity and causes of failure of well integrity barriers (A review). J. Nat. Gas Sci. Eng. 45, 511–526.

Le-Minous, J.C., Mutti, D., Bouvet, A., Unanue-Rodriguez, I., Chang, A., Massie, I., Xiao, E., Schnell, E., 2017. Permeability study of API class G and B cements considering seawater and WBM contamination. In: SPE/IADC Drilling Conference and Exhibition. Society of Petroleum Engineers.

Liu, X., Nair, S.D., Aughenbaugh, K.L., Juenger, M.C., van Oort, E., 2020. Improving the rheological properties of alkali-activated geopolymers using non-aqueous fluids for well cementing and lost circulation control purposes. J. Petrol. Sci. Eng. 195, 107555.

Mangadlao, J.D., Cao, P., Advincula, R.C., 2015. Smart cements and cement additives for oil and gas operations. J. Petrol. Sci. Eng. 129, 63–76.

Montserrat, S., 1993. Calorimetric measurement of the maximum glass transition temperature in a thermosetting resin. J. Therm. Anal. 40 (2), 553–563.

Moreira, P.H.S.S., de Oliveira Freitas, J.C., Braga, R.M., Araújo, R.M., de Souza, M.A.F., 2018. Production of carboxymethyl lignin from sugar cane bagasse: a cement retarder additive for oilwell application. Ind. Crop. Prod. 116, 144–149.

Nazir, R., Momeni, E., Armaghani, D.J., Amin, M.M., 2013. Correlation between unconfined compressive strength and indirect tensile strength of limestone rock samples. Electron. J. Geotech. Eng. 18 (1), 1737–1746.

Nelson, A.Z., Ewoldt, R.H., 2017. Design of yield-stress fluids: a rheology-to-structure inverse problem. Soft Matter 13 (41), 7578–7594.

Nelson, E.B., Guillot, D., 2006. Well Cementing. Schlumberger.

Norsok, D., 2013. Well integrity in drilling and well operations, 010 Standards Norway, Rev 4.

Paiva, M.D., Silva, E.C., Melo, D.M., Martinelli, A.E., Schneider, J.F., 2018. A geopolymer cementing system for oil wells subject to steam injection. J. Petrol. Sci. Eng. 169, 748–759.

Papadakis, V.G., Fardis, M.N., Vayenas, C.G., 1992. Hydration and carbonation of pozzolanic cements. Materials Journal 89 (2), 119–130.

Power, D., Zamora, M., 2003. Drilling Fluid Yield Stress: Measurement Techniques for Improved Understanding of Critical Drilling Fluid Parameters. AADE Technical Conference, Houston, pp. 1–3.
Saasen, A., Ytrehus, J.D., 2018. Rheological properties of drilling fluids: use of dimensionless shear rates in herschel-bulkley and power-law models. Appl. Rheol. 28 (5).
Salehi, S., Khattak, J., Saleh, F.K., Igbojekwe, S., 2019. Investigation of mix design and properties of geopolymers for application as wellbore cement. J. Petrol. Sci. Eng. 178, 133–139.
Santos, L., Dahi Taleghani, A., Li, G., 2018. Smart expandable polymer cement additive to improve zonal isolation. In: SPE/AAPG Eastern Regional Meeting. Society of Petroleum Engineers.
Santos, L., Dahi Taleghani, A., Li, G., 2020. Smart expandable fiber additive to prevent formation of microannuli. SPE Drilling & Completion.
Thomas, J., Musso, S., Catheline, S., Chougnet-Sirapian, A., Allouche, M., 2014. Expanding cement for improved wellbore sealing: prestress development, physical properties, and logging response. In: SPE Deepwater Drilling and Completions Conference. Society of Petroleum Engineers.
Todorovic, J., Raphaug, M., Lindeberg, E., Vrålstad, T., Buddensiek, M.-L., 2016. Remediation of leakage through annular cement using a polymer resin: a laboratory study. Energy Procedia 86, 442–449.
Tomosawa, F., Noguchi, T., 1993. Relationship between compressive strength and modulus of elasticity of high-strength concrete. In: Proceedings of the Third International Symposium on Utilization of High-Strength Concrete. Norwegian Concrete Assn Lillehammer, Norway, pp. 1247–1254.
Vignes, B., 2011. Contribution to Well Integrity and Increased Focus on Well Barriers in a Lifecycle Aspect. University of Stavanger.
Vrålstad, T., Saasen, A., Fjær, E., Øia, T., Ytrehus, J.D., Khalifeh, M., 2018. Plug & abandonment of offshore wells: ensuring long-term well integrity and cost-efficiency. J. Petrol. Sci. Eng.
Wagh, A.S., 2016. Chemically Bonded Phosphate Ceramics: Twenty-First Century Materials with Diverse Applications. Elsevier.